

Information-theoretical analysis of skyrmion dynamics at finite temperature in a box—a simulation study

Tenta Tani¹, Soma Miki²⁻⁵, Hiroki Mori², Minori Goto²⁻⁴, Yoshishige Suzuki²⁻⁴, Eiiti Tamura²

¹*Department of Physics, Osaka University, Toyonaka, Osaka 560-0043, Japan*

²*Graduate School of Engineering Science, Osaka University, Toyonaka, 560-8531, Japan*

³*Spintronics Research Network Division, Institute for Open and Transdisciplinary Research Initiatives, Osaka University, Suita, 565-0871, Japan*

⁴*Center for Spintronics Research Network (CSRN), Graduate School of Engineering Science, Osaka University, Toyonaka, 560-8531, Japan*

⁵*WPI Advanced Institute for Materials Research (AIMR), Tohoku University, Sendai, 980-8577, Japan*

(Dated: December 30, 2024)

We theoretically investigate the classical dynamics and flow of information in an interacting two-skyrmion system confined in a box at finite temperature. Using numerical simulations based on the Thiele-Langevin equation, we demonstrate that the skyrmion motion cannot be fully described by the master equation, highlighting the system’s simplicity with its nontrivial dynamics. Through the analysis of information-theoretical quantities, we elucidate the physical significance of transfer entropy as a measure of information flow. Notably, the peak position of the transfer entropy, as a function of time delay, is found to be independent of the interaction range between the two skyrmions yet dependent on the box size. This peak corresponds to the characteristic time required for changing the skyrmion state: the box size divided by the average velocity of skyrmions. We can understand that the information transmission time consists of the time to obtain mutual information and the time to write the information.

I. INTRODUCTION

Information theory and physics are becoming increasingly interconnected, with one actively studied area being information thermodynamics [1–10]. Information thermodynamics highlights the equivalence of information and energy (or work), as demonstrated by the resolution of Maxwell’s demon paradox [5–9, 11–14]. Mutual information, an information-theoretical quantity, is associated with work, while transfer entropy [15], a type of mutual information, serves as a measure of information flow [16–31].

It is used to analyze the information flow in various systems and time series, including neural systems [16–19] and stock markets [21–23]. For example, Schreiber [15] introduced transfer entropy and used it to examine the information flow between heartbeat and breathing, revealing a stronger information flow from the heart rate to the breathing rate than that in the reverse direction, as indicated by its higher transfer entropy.

Although the transfer entropy has been mainly applied to complex systems and time series, its significance in simpler physical systems remains unclear. For instance, in systems of interacting particles, the exact relationship between the transfer entropy and particle dynamics is unknown. Key questions include: how can we define the information flow between particles, and how is information transferred through particle collisions? Addressing these questions in simpler systems can clarify the physical meaning of transfer entropy, enabling the application of information flow concepts to physical systems such as nanoparticles in liquids and molecules in gases. Ultimately, studying the transfer entropy in these systems

is essential for advancing the interdisciplinary field connecting information theory and physics.

The skyrmion system [32–35] is ideal for studying information flow. Skyrmions exhibit Brownian motion [36–44], interact repulsively with one another [44–46], and can be confined in an energetic box [42–44]. Stochastic Brownian motion enables information-theoretical analysis, while the repulsive interactions between skyrmions allow investigation of the information flow. The skyrmion system has already been experimentally realized in a confined box [42–44] and are promising for ultralow-power Brownian computing [13, 38, 47]. Therefore, understanding the nature of information flow in skyrmion systems is valuable in fundamental and applied research.

In this study, we investigated a two-skyrmion system confined in a box at a finite temperature using the Thiele-Langevin equation as a theoretical model. The analysis demonstrated that the simulated probability distribution cannot be reproduced by the master equation, indicating nontrivial skyrmion dynamics. Examination of the transfer entropy $T(\Delta t)$ between “the first skyrmion at time t ” and “the second skyrmion at time $t - \Delta t$ ”, demonstrated that the functional shape of $T(\Delta t)$ exhibits a peak structure. The analysis also revealed that the peak position depends only on the box size but not on the skyrmion-skyrmion interaction range, suggesting that the transfer entropy peak corresponds to the time interval required for a skyrmion to influence another skyrmion through repulsive interactions—representing the information transmission time. Notably, we can understand that the information transmission time consists of the time to obtain mutual information and the time to write the information. Owing to the simplicity of the system, these novel

results on the nature of information flow were revealed. This is because previous research has focused on complex systems, where it is difficult to deeply analyze and understand the physical significance of transfer entropy.

This paper is organized as follows. Sec. II presents the theoretical model for examining the two-skyrmion system, introduces the Thiele-Langevin equation and discusses skyrmion interactions. Sec. III focuses on the skyrmion system dynamics, demonstrating their simplicity and nontriviality. Sec. IV explores several information-theoretical measures, including the transfer entropy to investigate the information flow between two skyrmions. Sec. V concludes the study.

II. MODEL OF INTERACTING SKYRMIONS IN A BOX

In this study, we considered the classical motion of skyrmions. The dynamics of two interacting skyrmions in a potential box are governed by a stochastic differential equation called the Thiele-Langevin equation [37, 48, 49],

$$\begin{aligned} m \frac{d\mathbf{v}_1}{dt} &= -\alpha D \mathbf{v}_1 + \mathbf{G} \times \mathbf{v}_1 + \mathbf{F}_{\text{int}}(\mathbf{r}_1, \mathbf{r}_2) + \mathbf{F}_{\text{wall}}(\mathbf{r}_1) + \mathbf{R}_1, \\ m \frac{d\mathbf{v}_2}{dt} &= -\alpha D \mathbf{v}_2 + \mathbf{G} \times \mathbf{v}_2 - \mathbf{F}_{\text{int}}(\mathbf{r}_1, \mathbf{r}_2) + \mathbf{F}_{\text{wall}}(\mathbf{r}_2) + \mathbf{R}_2, \end{aligned} \quad (1)$$

where \mathbf{r}_j , \mathbf{v}_j are the two-dimensional position and velocity of the j -th skyrmion ($j = 1, 2$), respectively, and $m = 1.0 \times 10^{-22}$ kg is the skyrmion mass [37, 41, 49–51]. In this study, mass is treated as a parameter. As presented later in Sec. IV, the relative values are important because the time constant depends on the mass; except at equilibrium, where each result is mass-independent. Thermal fluctuation-induced mass also exists [51] in the system; however, it is negligible compared to the motion-induced mass in the potential [49, 50]; therefore, only the latter is considered in this study. For the friction term $-\alpha D \mathbf{v}_j$, $\alpha = 0.02$ is Gilbert constant, and $D = 7.06 \times 10^{-14}$ kg/s is dissipation dyadic, with D dependent on the skyrmion radius $R = 25.55$ nm and domain wall width $w = 11.35$ nm [52–56]. In the second term, $\mathbf{G} = -G \hat{\mathbf{z}}$ is the gyrocoupling vector [39–41] where $G = 4.97 \times 10^{-14}$ kg/s.

We modeled the skyrmion interaction using an exponentially decaying interaction when the two skyrmions are apart, whereas a constant force upon contact expressed as

$$\mathbf{F}_{\text{int}}(\mathbf{r}_1, \mathbf{r}_2) = \begin{cases} F_0(\mathbf{r}_{12}/r_{12})e^{-(r_{12}-R)/\xi} & (r_{12} > R) \\ F_0(\mathbf{r}_{12}/r_{12}) & (r_{12} < R), \end{cases} \quad (2)$$

where $r_{12} = |\mathbf{r}_1 - \mathbf{r}_2|$. $F_0 = 1.0 \times 10^{-11}$ N is the magnitude and ξ is the interaction range. For computational simplicity, this interaction was modeled as a short-range exchange interaction, neglecting the dipole interaction due to the small skyrmion radius of order 10^{-9} m.

The force exerted by the walls of the square box is modeled using exponentially decaying potential energy,

$$\mathbf{F}_{\text{wall}}(\mathbf{r}) = -\nabla U_{\text{wall}}(\mathbf{r}), \quad (3)$$

where the potential $U_{\text{wall}}(\mathbf{r})$ is expressed as,

$$U_{\text{wall}}(\mathbf{r}) = U_0 \left[e^{-(x+\tilde{d})/\xi_0} + e^{(x-\tilde{d})/\xi_0} + e^{-(y+\tilde{d})/\xi_0} + e^{(y-\tilde{d})/\xi_0} \right], \quad (4)$$

where \tilde{d} is a parameter representing the size of the box. In this equation, the magnitude U_0 was set to $U_0 = 1.0 \times 10^{-20}$ J and $\xi_0 = 8.52$ nm to fit the results given by the analytical formula [52, 57] (see Appendix B). As shown in Fig. 1, the side of the box is $2d$. The box size $d = 5.69R$ corresponds to the parameter $\tilde{d} = 3R$.

The last term \mathbf{R}_j in Eq. (1) is a random force originating from thermal fluctuations. This force is determined through the fluctuation-dissipation theorem,

$$[\mathbf{R}_j]_\alpha = \sqrt{\frac{2\alpha D k_B T}{\delta t}} \mathcal{N}(0, 1) \quad (\alpha = x, y), \quad (5)$$

where δt is a time increment and $\mathcal{N}(0, 1)$ stands for the standard normal distribution, k_B is the Boltzmann constant, and T is the temperature of the system. Hereafter, we set $T = 300$ K.

III. SKYRMION DYNAMICS

By solving the Thiele-Langevin equation [Eq. (1)], we have derived the trajectories of the two skyrmions. Fig. 1(a) illustrates a snapshot of their motions, with the orange and green circles representing the first skyrmion labeled “skyrmion X ” and the second skyrmion labeled “skyrmion Y ”, respectively. The box size was set to $d = 5.69R$. To information-theoretically analyze the dynamics of skyrmions in Sec. IV, the skyrmions positions were discretized into four cells: cells 0–3 [see Fig. 1(a)]. Fig. 1(b) illustrates the trajectories of the two skyrmions, illustrating confinement within the box and mutual repulsion. Furthermore, the clockwise cyclotron motion caused by the gyrocoupling term $\mathbf{G} \times \mathbf{v}$ [see Eq. (1)] is analogous to the Lorentz force on an electron in a magnetic field. We based the analysis on $N \approx 10^5$ simulations, which are sufficient to minimize statistical errors. Throughout this study, we used a time increment $\delta t = 1$ ns and a simulation time $t_f = 1000$ ns. In Sec. III A, we consider a single skyrmion system, followed by an interacting two-skyrmion system in Sec. III B.

A. One-body system

First, we consider a single skyrmion in the box. We denote the discretized position of the skyrmion at time t in

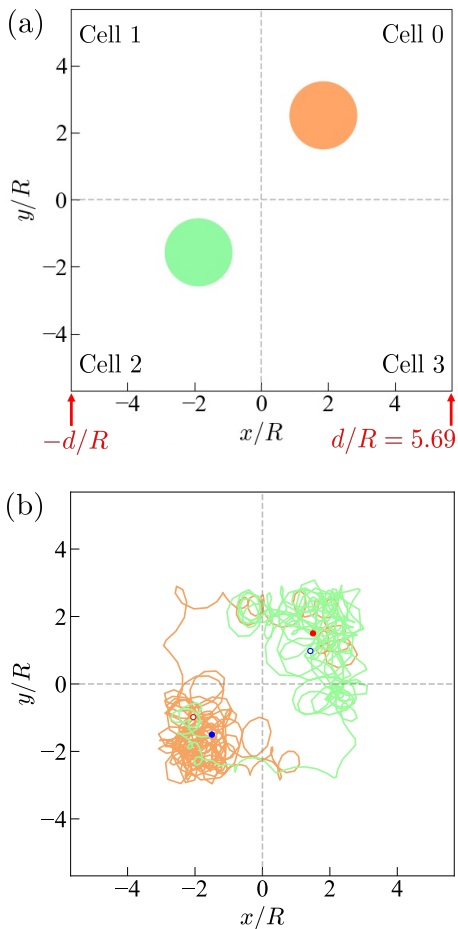


FIG. 1. (a) Snapshot of the two skyrmions drawn by the orange and green circles with radius R , in a square box. The box is divided into the four cells (cell 0, 1, 2, and 3). (b) Trajectories of the two skyrmions. For the orange (green) skyrmion, the initial and final point is shown by the filled and open red (blue) circle, respectively. We see the clockwise cyclotron motion and the counterclockwise skipping trajectory.

i -th simulation as $x_t^{(i)} = 0, 1, 2, 3$. Numerical calculations yield N time series

$$(x_0^{(i)}, x_{\delta t}^{(i)}, x_{2\delta t}^{(i)}, \dots, x_{t_f}^{(i)}), \quad i = 1, 2, \dots, N. \quad (6)$$

At each time t , the state of the skyrmion was treated as a stochastic variable X_t . The probability that a skyrmion exists in cell x_t at time t is given by

$$p(x_t) = \frac{1}{N} \sum_{i=1}^N \delta(x_t^{(i)} - x_t), \quad (7)$$

where $\delta(x)$ is Kronecker's delta,

$$\delta(x) = \begin{cases} 1 & (x = 0) \\ 0 & (x \neq 0). \end{cases} \quad (8)$$

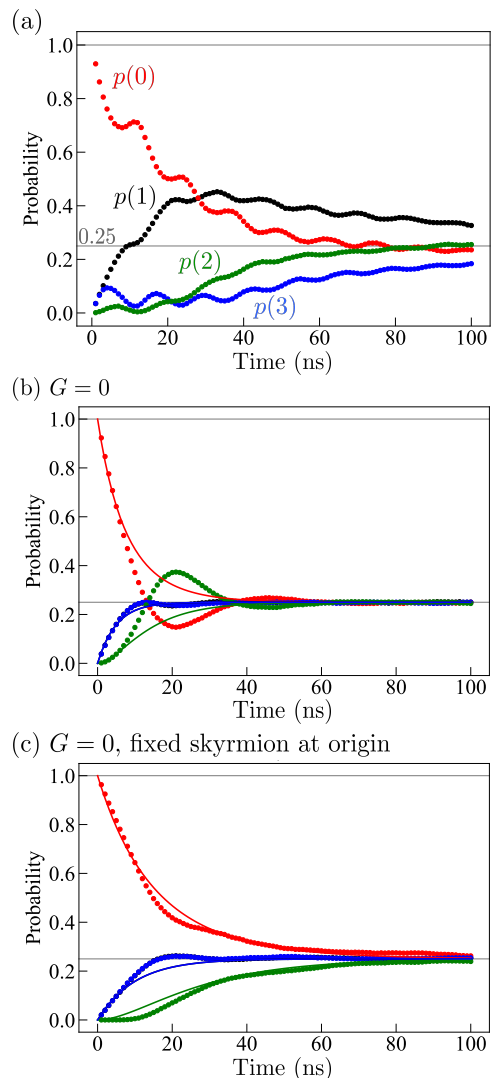


FIG. 2. Time evolution of the occupation probabilities $p(x_t)$ for $x_t = 0, 1, 2, 3$ (red, black, green, and blue, respectively) for (a) single skyrmion, (b) single skyrmion with $G = 0$, and (c) single moving skyrmion and fixed skyrmion at the origin, with $G = 0$. The dots are the simulated results, and the solid curves are the analytical solutions of the master equation. The gray horizontal line indicates $p = 0.25$, to which all probabilities converge in $t \rightarrow \infty$ limit.

Similarly, the joint probability between different times t and t' is written as

$$p(x_t, x_{t'}) = \frac{1}{N} \sum_{i=1}^N \delta(x_t^{(i)} - x_t) \delta(x_{t'}^{(i)} - x_{t'}), \quad (9)$$

and the conditional probability can be obtained by Bayes' theorem: $p(x_t | x_{t'}) = p(x_t, x_{t'}) / p(x_{t'})$.

Based on this formulation, we investigated the time evolution of the probability $p(x_t)$ as illustrated in Fig. 2(a). The red, black, green, and blue dots correspond to $p(0), p(1), p(2)$, and $p(3)$, respectively. With

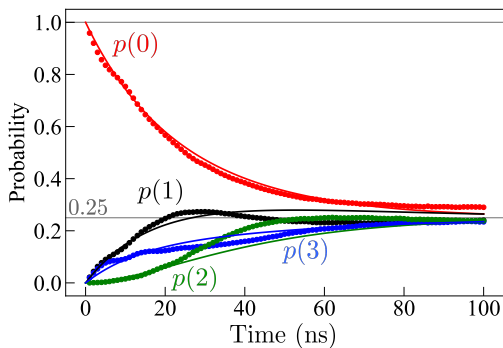


FIG. 3. Time evolution of the occupation probabilities $p(x_t)$ for $x_t = 0, 1, 2, 3$ (red, black, green, and blue, respectively) for the two-skyrmion system. The dots are the result of the simulation, and the solid lines are given from the analytical solutions of the master equation ($w = 0.02$ and $w' = 0.012$).

initial condition fixed at $x_0 = 0$, $p(0)$ rapidly decreases from $p(0) = 1$ to $p(0) = 0.25$ [red dots, Fig. 2(a)]. The wavy probability profiles result from the clockwise cyclotron motions induced by the gyrocoupling term $\mathbf{G} \times \mathbf{v}$, with the oscillation frequency matching the cyclotron frequency $\omega = G/m$. The asymmetry between $p(1)$ (black dots) and $p(3)$ (blue dots) was attributed to the skipping trajectory along the walls. This skipping is simply an edge current accompanied by cyclotron motion; thus, its direction is counterclockwise.

When G is turned off, probabilities evolve as illustrated in Fig. 2(b). Without chiral motion, $p(1) = p(3)$ at all times (overlapping black and blue dots). Notably, near $t = 20$ ns, $p(2)$ (green dots) temporarily exceeds $p(0)$ (red dots) which is a nontrivial overshoot behavior that cannot be reproduced by the results obtained using the master equation [solid curves in Fig. 2(b)]. For the curve fitting, we used the transition rate parameters $w = w' = 0.05$. A detailed description of the master equation and its analytical solution is provided in Appendix A. The nontrivial overshooting behavior in Fig. 2(b) is caused by the singularity of the origin. As illustrated in Fig. 2(c), fixing the skyrmion at the origin eliminates the overshoot, allowing the master equation to qualitatively match the dynamics with $w = w' = 0.025$ (see Appendix A). Moreover, if the square box is divided into two cells, the master equation reproduces the simulated probability distribution very well (data not shown); however, overshooting persists without a skyrmion fixed at the origin.

B. Two-body system

For the rest of this study, we consider two interacting skyrmions confined in a box. The time evolution of the occupation probability $p(x_t)$ is shown in Fig. 3. As illustrated in Fig. 2(a), skyrmion-skyrmion interactions sup-

press the oscillatory behavior in the single-skyrmion case. Similarly, in the two-skyrmion case, the master equation curve fit was also unsuccessful in capturing the behavior of the system (solid curves in Fig. 3), with parameters $w = 0.02$ and $w' = 0.012$ (see Appendix A).

The results from this section demonstrate that skyrmions in a box are simple yet have nontrivial system dynamics.

IV. INFORMATION-THEORETICAL ANALYSIS USING ENTROPIC QUANTITIES

In this section, we analyze the motions of the two skyrmions using entropic quantities to investigate the nature of the transfer entropy. Let X_t, Y_t be the stochastic variables of the skyrmion X and Y at time t , respectively. The Shannon entropy of skyrmion X at time t is written as

$$H(X_t) = - \sum_{x_t} p(x_t) \ln p(x_t), \quad (10)$$

which quantifies the randomness of the motion of the skyrmion X . Similarly, we can calculate the conditional Shannon entropy between X_t and $Y_{t-\Delta t}$ using

$$H(X_t|Y_{t-\Delta t}) = - \sum_{x_t, y_{t-\Delta t}} p(x_t, y_{t-\Delta t}) \ln p(x_t|y_{t-\Delta t}). \quad (11)$$

Fig. 4(a) illustrates the time evolution of Shannon entropy $H(X_t)$ in units of $\ln 4$ for various interaction ranges ξ . The black, red, blue, green, and yellow curves correspond to ranges $\xi/\xi_0 = 2.0, 2.5, 3.0, 3.5$, and 4.0 , respectively, while the gray dots represent the case of a free skyrmion (no interaction). The box size is fixed at $d/R = 5.69$. Due to symmetry, $H(X_t) = H(Y_t)$. In all cases, the Shannon entropy converges to the equilibrium state ($H = \ln 4$) for $t > 800$ ns. The skyrmion-skyrmion interaction delays relaxation to the equilibrium state, thus cases with longer interaction range ξ are slower in reaching equilibrium.

To quantify the correlation between the two skyrmions, we used the mutual information

$$I(X_t : Y_{t-\Delta t}) = H(X_t) - H(X_t|Y_{t-\Delta t}), \quad (12)$$

which consists of the Shannon entropy and conditional Shannon entropy. Mutual information $I(X_t : Y_{t-\Delta t})$ represents the information shared between skyrmion X at time t (X_t) and skyrmion Y at time $t - \Delta t$ ($Y_{t-\Delta t}$). At large time delays Δt , X_t and $Y_{t-\Delta t}$ become uncorrelated such that $H(X_t|Y_{t-\Delta t}) = H(X_t)$ and $I(X_t : Y_{t-\Delta t}) = 0$, indicating no shared information. In Fig. 4(b), $I(X_t : Y_{t-\Delta t})$ is illustrated as a function of the time delay Δt under the same condition as in Fig. 4(a). To consider the equilibrium states, we set $t = t_f = 1000$ ns. For all interaction ranges ξ , the mutual information decreases monotonically with increasing Δt , as the equal-time correlation at

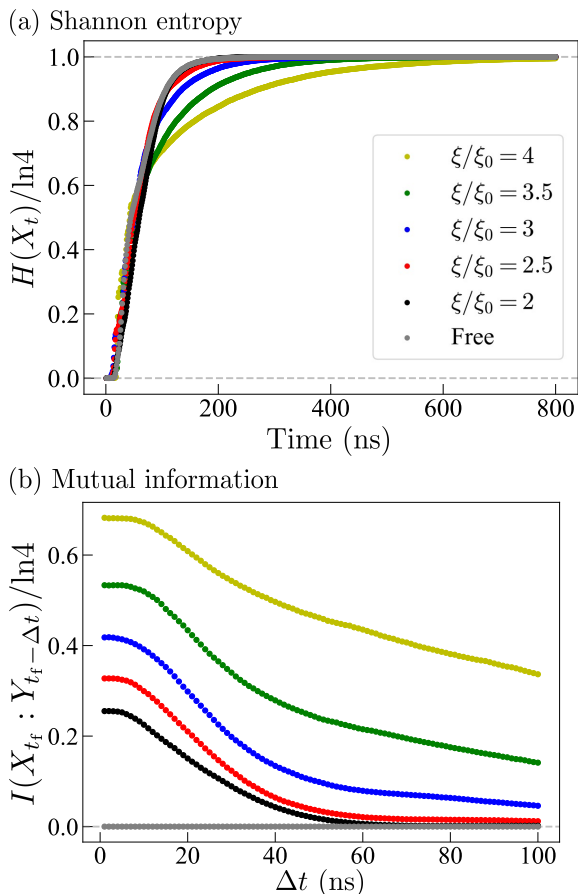


FIG. 4. (a) Shannon entropy $H(X_t)$ of the skyrmion in units of $\ln 4$. The different colors (black, red, blue, green, and yellow) correspond to several interaction ranges $\xi/\xi_0 = 2.0, 2.5, 3.0, 3.5$, and 4.0 , respectively. The gray plots are for the non-interacting case (free skyrmion). (b) Mutual information $I(X_t : Y_{t-\Delta t})$ is plotted as a function of the time delay Δt , in the same manner as (a).

$\Delta t = 0$ diminishes due to Brownian motion. Stronger interactions (larger ξ) result in greater mutual information, while free skyrmions (gray dots) demonstrate no mutual information. These results confirm that $I(X_t : Y_{t-\Delta t})$ does not represent the flow of information between two skyrmions.

To explore the directional flow of information, we investigated the transfer entropy

$$\begin{aligned} T_{Y \rightarrow X}(\Delta t) &= I(X_t : Y_{t-\Delta t} | X_{t-\Delta t}) \\ &= H(X_t | X_{t-\Delta t}) - H(X_t | X_{t-\Delta t}, Y_{t-\Delta t}), \end{aligned} \quad (13)$$

which is a widely used measure of information flow [16–31]. Fig. 5(a) shows the calculated transfer entropy $T_{Y \rightarrow X}(\Delta t)$ as a function of the time delay Δt for various interaction ranges $\xi = 2.0, 2.5, 3.0, 3.5$, and 4.0 , with t fixed at $t_f = 1000$ ns and $d/R = 5.69$. Unlike the mutual information illustrated in Fig. 4(b), the transfer entropy exhibits a pronounced peak structure. Notably,

the peak positions remain nearly unchanged across all interaction ranges ξ . As ξ increases, the peak magnitude of the transfer entropy generally grows, except for $\xi/\xi_0 = 4.0$ (yellow). In the extreme case of $\xi/\xi_0 = 4.0$, the two skyrmions become less active. Due to the extended interaction range, the skyrmions experienced strong repulsion even when they were far apart and located near a corner. Consequently, the skyrmions tend to reside in stable cells (e.g., cell 0 and 2), thereby suppressing the peak value of the transfer entropy. In addition to transfer entropy, we consider active information storage [58],

$$A_X(\Delta t) = I(X_t : X_{t-\Delta t}), \quad (14)$$

which can be regarded as the transfer entropy between the skyrmion X and itself. Fig. 5(b) shows $A_X(\Delta t)$ at $t = t_f$ as a function of Δt . Unlike the previous form of transfer entropy, $A_X(\Delta t)$ exhibits no peak structures, indicating a monotonous memory loss due to the random motion of the skyrmion. However, the forgetting speed is slower for longer interaction ranges ξ , because stronger interactions suppress random cell transitions. Notably, the wavy structure of the interaction-free skyrmion (gray) arises from the cyclotron motion (see Sec. III), which vanishes in interacting cases. Together, Figs. 5(a) and (b) reveal that the transfer entropy peak originates purely from the skyrmion-skyrmion interactions.

Moreover, the impact of box size is examined for $\xi/\xi_0 = 2$, as illustrated in Figs. 5(c) and (d) which present the results for transfer entropy and active information storage, respectively. Small ($\tilde{d} = 2R$), medium ($\tilde{d} = 3R$), and large ($\tilde{d} = 4R$) boxes are represented by the rhombus, circle, and square dots, respectively. In Fig. 5(c), unlike in Fig. 5(a), the peak positions of $T_{Y \rightarrow X}(\Delta t)$ shift depending on the box size d ; larger box sizes d lead to later peak time. For the large box, cyclotron motion becomes evident as the two skyrmions are free to move at the corners of the box. In Fig. 5(d), the active information storage continues to monotonously decay, similar to Fig. 5(b). Compared with the case of the medium-size box (filled circles), the skyrmions in the smaller box (rhombus dots) lose their memory more slowly. Skyrmions confined in the smaller box interact more strongly each other and tend to remain in the same stable configuration (e.g. cell 0 and 2). In the large box (square dots), the forgetting speed is slower than the medium-size box (filled circles), because the two skyrmions tend to move freely near the corners.

Comparing the mutual information [Fig. 4(b)] and the transfer entropy [Fig. 5(a)] for several ξ , we find that the mutual information starts to decrease at certain time, which is earlier than the transfer entropy peak. This is because mutual information represents the shared information between skyrmion X and Y : whichever skyrmion randomly moves, the mutual information drops. Additionally, note that the shoulder of the mutual information [Fig. 4(b)] becomes longer as ξ increases, demonstrating that stronger interaction contributes to keep the shared information between the skyrmions.

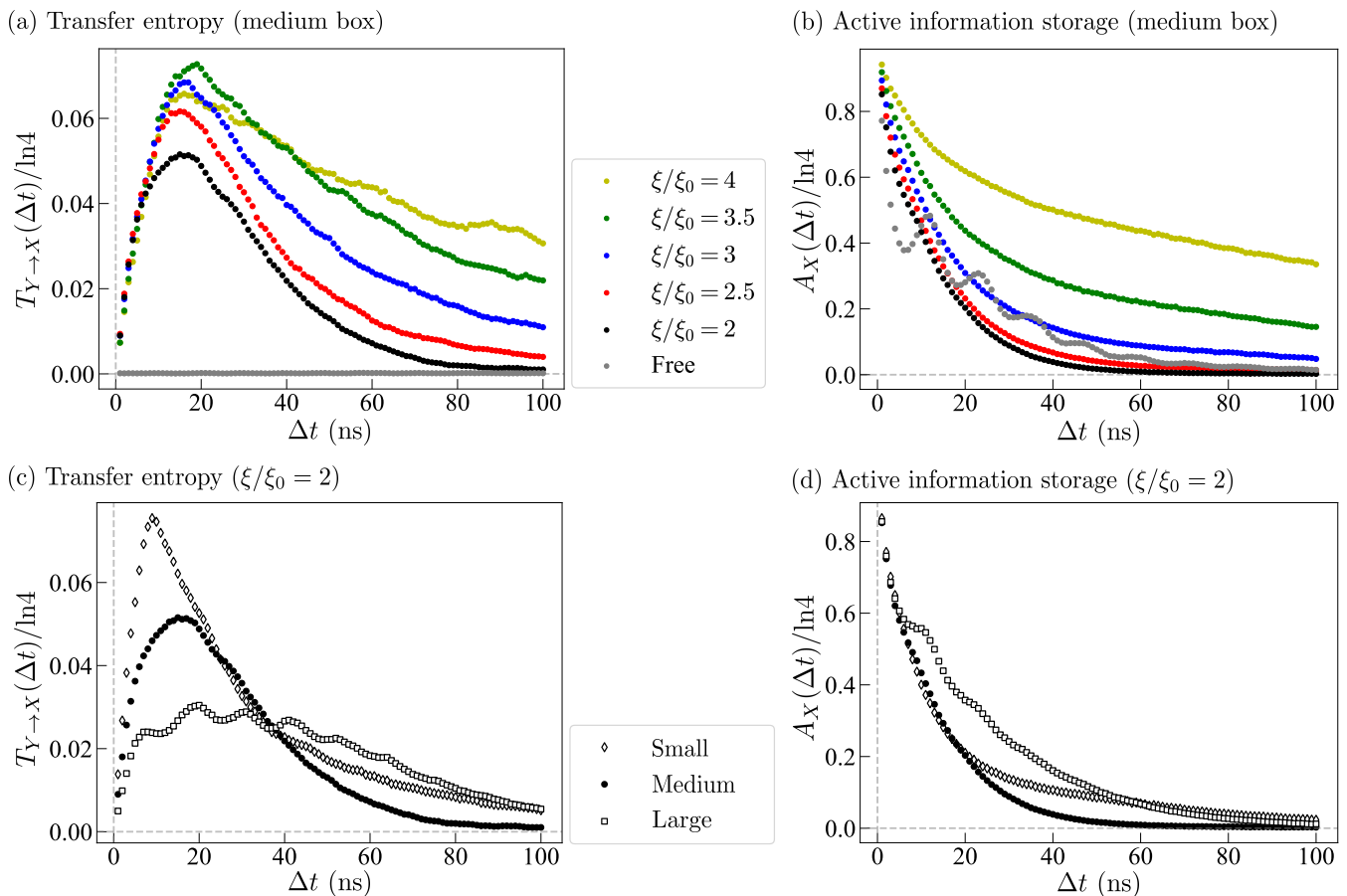


FIG. 5. For various interaction ranges $\xi/\xi_0 = 2.0, 2.5, 3.0, 3.5,$ and 4.0 , (a) the transfer entropy and (b) the active information storage are plotted as a function of the time delay Δt , where the box size $d/R = 5.69$ (medium size). The meaning of the different colors is the same as Fig. 4. (c) and (d) are the same plots for the three different box sizes. The respective small, medium, and large boxes correspond to rhombus, circle, and square dots. The interaction range $\xi/\xi_0 = 2$.

From these results, the transfer entropy peak position can be interpreted as the time required for state transitions driven by skyrmion-skyrmion interaction. For example, if skyrmion X is located in cell 0 and skyrmion Y in cell 2 (a stable state), a random force might accidentally move Y to cell 3, prompting X to shift to cell 1 due to repulsive interactions. However, these state transitions ($Y : 2 \rightarrow 3$ and $X : 0 \rightarrow 1$) do not occur instantaneously but occur in finite time, which depends on the box size d . Smaller boxes enable faster state transitions, resulting in earlier transfer entropy peaks. This interval represents the information transmission time necessary for one skyrmion to influence the other. Since the peak position is unchanged when we vary interaction ranges ξ , we can understand information transmission time consists of the time to obtain mutual information and the time to write the information. In our two-skyrmion system, mutual information exists from the beginning, therefore the information transmission time is equal to the writing time of information. In fact, the transfer entropy peak positions, which depend on the box size d , are qualitatively

reproduced using the transition time between adjacent cells by diffusion.

V. CONCLUSION

We theoretically investigated the dynamics of a two-skyrmion system confined in a box at a finite temperature and examined the nature of the transfer entropy in the system. Numerical solutions to the Thiele-Langevin equation indicated that skyrmion dynamics are nontrivial, although this system consists only of two particles. This complexity arises from the chiral motion of skyrmions resulting from the gyrocoupling term $\mathbf{G} \times \mathbf{v}$. By calculating the Shannon entropy, mutual information, active information storage, and transfer entropy, we elucidated the physical meaning of transfer entropy. The transfer entropy peak position is independent of the interaction range between the two skyrmions, but is dependent on the box size. Thus, the transfer entropy peak signifies the time interval required for one parti-

cle to influence the other particle's state, representing the information transmission time. Contrary to expectations, we showed that the speed of information transfer is unaffected by the interaction strength ξ . Information transmission time can be understood as the sum of the time to obtain mutual information and the time to write the information. This work provides a deeper understanding of transfer entropy and demonstrates the value of information-theoretical analyses in physical systems. Furthermore, these findings could be important to consider a future application such as the ultralow power Brownian computing using the information flow between skyrmions. This study bridges the gap between the conceptual understanding of transfer entropy in complex systems and its application to simpler physical systems, thereby strengthening the connection between information theory and physics.

classical master equation is written as

$$\frac{d\mathbf{p}}{dt} = A\mathbf{p},$$

$$A = -(w + w' + w'')I + \begin{pmatrix} 0 & w' & w'' & w \\ w & 0 & w' & w'' \\ w'' & w & 0 & w' \\ w' & w'' & w & 0 \end{pmatrix}, \quad (\text{A1})$$

$$\mathbf{p} = \begin{pmatrix} p(0) \\ p(1) \\ p(2) \\ p(3) \end{pmatrix},$$

where I is a 4×4 identity matrix. The parameters w, w' , and w'' represents the transition rate between the cells $0 \rightarrow 1$, $0 \rightarrow 3$, and $0 \rightarrow 2$, respectively. When the smallest parameter w'' was turned off, we were able to solve the equation analytically:

$$\begin{pmatrix} p(0) \\ p(1) \\ p(2) \\ p(3) \end{pmatrix} = \frac{1}{4} \left[\begin{pmatrix} 1 \\ 1 \\ 1 \\ 1 \end{pmatrix} + \begin{pmatrix} 1 \\ -1 \\ 1 \\ -1 \end{pmatrix} e^{-2w_+t} + \begin{pmatrix} \cos w_-t \\ \sin w_-t \\ -\cos w_-t \\ -\sin w_-t \end{pmatrix} e^{-w_+t} \right], \quad (\text{A2})$$

where $w_{\pm} = w \pm w'$. We assume the initial condition $\mathbf{p} = (1, 0, 0, 0)^T$ at $t = 0$. In Figs. 2 and 3, we fitted the simulated results using this analytical form. Note that the inclusion of w'' does not largely alter the result.

Appendix A: Analytical solution of the master equation

In this appendix, we present details of the analysis using the master equation shown in Figs. 2 and 3. The

Appendix B: Analytical formula for energetic box

In this section, we evaluate the validity of modeling the force from the potential barrier to the skyrmion. In this study, we considered barriers that confine skyrmion using a confinement-efficient magnetic anisotropy energy step [52, 57]. The potential $U_{\text{ani}}(X)$ of a skyrmion at a distance of X from the wall owing to the magnetic anisotropy energy step and the force $\mathbf{F}_{\text{ani-wall}}$ from the energy barrier obtained from this potential $U_{\text{ani}}(X)$ are respectively described in the following equations [52]

$$U_{\text{ani}}(X) = -\Delta Kt \int_{-\infty}^{\infty} \int_0^X dx dy (1 - m_z^2(\mathbf{r})) + \frac{K_{\text{wall}} + K_{\text{cell}}}{2} t \int_{-\infty}^{\infty} \int_{-\infty}^{\infty} dx dy (1 - m_z^2(\mathbf{r}))$$

$$= -2\Delta Kt \int_0^{\infty} \int_0^X dx dy \frac{4 \sinh^2(R/w) \sinh^2(\sqrt{x^2 + y^2}/w)}{[\sinh^2(R/w) + \sinh^2(\sqrt{x^2 + y^2}/w)]^2}$$

$$+ 2(K_{\text{wall}} + K_{\text{cell}})t \int_0^{\infty} \int_0^{\infty} dx dy \frac{4 \sinh^2(R/w) \sinh^2(\sqrt{x^2 + y^2}/w)}{[\sinh^2(R/w) + \sinh^2(\sqrt{x^2 + y^2}/w)]^2}, \quad (\text{B1})$$

$$F_{\text{ani-wall}}(X) = -\Delta Kt \int_{-\infty}^{\infty} dy \frac{4 \sinh^2(R/w) \sinh^2(\sqrt{x^2 + y^2}/w)}{[\sinh^2(R/w) + \sinh^2(\sqrt{x^2 + y^2}/w)]^2}, \quad (\text{B2})$$

where t and $m_z(\mathbf{r})$ are the thickness of the ferromagnetic

film and the z -component of the magnetization at po-

sition $\mathbf{r} = (x, y) = (r \cos \varphi, r \sin \varphi)$, respectively. K_{wall} and K_{cell} are the magnetic anisotropy at the potential barrier and the cell, respectively. $\Delta K = K_{\text{wall}} - K_{\text{cell}}$ is the height of the magnetic anisotropy energy step. The skyrmion profiles are described by the functions modeled in Ref. [54]. The second term of $U_{\text{ani}}(X)$ is a constant, and therefore does not contribute to the force $F_{\text{ani-wall}}$. Because this function is complex and requires an enormous amount of time to simulate, an exponential model function [Eq. (4)] was used. Figure 6(a) shows the potential $U_{\text{ani}}(X)$ [Eq. (B1), blue curve] and the model function U_{wall} [Eq. (4), orange curve]. Fig. 6(c) shows the force $F_{\text{ani-wall}}$ from the wall [Eq. (B2), blue curve] and the model function F_{wall} [Eq. (3), orange curve]. Figure 6(b) and (d) are the enlarged views of (a) and (c), respectively. The potential $U_{\text{ani}}(X)$ and force $F_{\text{ani-wall}}$ from the wall shown in Fig. 6 correspond to $K_{\text{cell}} = 0.9 \text{ MJ/m}^3$,

$K_{\text{wall}} = 1.15K_{\text{cell}} = 1.035 \text{ MJ/m}^3$, and $t = 1.2 \text{ nm}$. In Fig. 6(b), the red dashed line represents the value of $3k_{\text{B}}T$ at 300 K, which means that the skyrmions are confined within a standard deviation of 3σ in the cell. In the region $X > 1.61R$, the model functions for the potential and force were fitted to the analytical equations $U_{\text{ani}}(X)$ and $F_{\text{ani-wall}}$. These model functions only consider the direction perpendicular to the wall and do not include the contribution from the wall at the corners of the cell. Therefore, the effects of the corners are evaluated below. Fig. 7(a) shows the coordinate system of the cell corner rotated by $\pi/4$ from the coordinate system in the main text. The gray area represents the potential barrier, while the white area represents the cell interior. In general, the formula for a potential with a corner of angle α is

$$\begin{aligned} U_{\text{ani}}(X) &= -2\Delta Kt \int_0^\alpha d\varphi \int_0^\infty r dr (1 - m_z^2(\mathbf{r})) + 2K_{\text{wall}}t \int_0^\pi d\varphi \int_0^\infty r dr (1 - m_z^2(\mathbf{r})) \\ &= -2\Delta Kt \int_0^\alpha d\varphi \int_0^\infty r dr \frac{4 \sinh^2(R/w) \sinh^2(\sqrt{r^2 + X^2 - 2rX \cos \varphi/w})}{[\sinh^2(R/w) + \sinh^2(\sqrt{r^2 + X^2 - 2rX \cos \varphi/w})]^2} \\ &\quad + 2K_{\text{wall}}t \int_0^\pi d\varphi \int_0^\infty r dr \frac{4 \sinh^2(R/w) \sinh^2(\sqrt{r^2 + X^2 - 2rX \cos \varphi/w})}{[\sinh^2(R/w) + \sinh^2(\sqrt{r^2 + X^2 - 2rX \cos \varphi/w})]^2}. \end{aligned} \quad (\text{B3})$$

Furthermore, the force f_α acting on the corner is

$$\begin{aligned} f_\alpha(X) &= -\Delta Kt \int_0^\alpha d\varphi \int_0^\infty r dr \frac{1}{w} \frac{X - r \cos \varphi}{\sqrt{r^2 + X^2 - 2rX \cos \varphi}} \frac{4 \sinh^2(R/w) \sinh(2\sqrt{r^2 + X^2 - 2rX \cos \varphi/w})}{[\sinh^2(R/w) + \sinh^2(\sqrt{r^2 + X^2 - 2rX \cos \varphi/w})]^2} \\ &\quad \times \left[1 - \frac{2 \sinh^2(\sqrt{r^2 + X^2 - 2rX \cos \varphi/w})}{\sinh^2(R/w) + \sinh^2(\sqrt{r^2 + X^2 - 2rX \cos \varphi/w})} \right]. \end{aligned} \quad (\text{B4})$$

Figure 7(b) shows the dependence of distance from the corner X_c to the force in the coordinate system in (a). The blue and green solid curves represent the forces $f_{\pi/2}$ and $f_{3\pi/4}$, respectively, and the black dotted curve represents the difference between $f_{\pi/2}$ and $f_{3\pi/4}$. The orange curve represents the model function F_{wall} . $f_{\pi/2}$ and F_{wall} take the factor $\sqrt{2}$, because the coordinates were transformed from Eq. (3) by angle $\pi/4$. Figure 7(c) is the ratio of $f_{\pi/2}$ to $\sqrt{2}f_{\pi/2} - f_{3\pi/4}$, which was used to evaluate the contribution of the corner barrier. The force

ratio is less than 10^{-2} in the region $X_c/w > 5.15$, i.e., $X > 1.61R$, and the corner components were very small, except for the gray regions in Fig. 6(b) and (d). Therefore, to reduce the simulation time, we evaluated various information flows in the region $X > 1.61R$ using a simple model function in Eqs. (3) and (4), respectively.

ACKNOWLEDGMENTS

This work was supported by JSPS KAKENHI Grant Numbers JP23KJ1497, JP20H05666, and JP24K22860, and by JST CREST Grant Number JPMJCR20C1, Japan.

-
- [1] J. M. Parrondo, J. M. Horowitz, and T. Sagawa, Thermodynamics of information, *Nat. Phys.* **11**, 131 (2015).
 [2] D. Andrieux and P. Gaspard, Nonequilibrium generation

- of information in copolymerization processes, *Proc. Natl. Acad. Sci. USA* **105**, 9516 (2008).
 [3] C. Jarzynski, The thermodynamics of writing a random

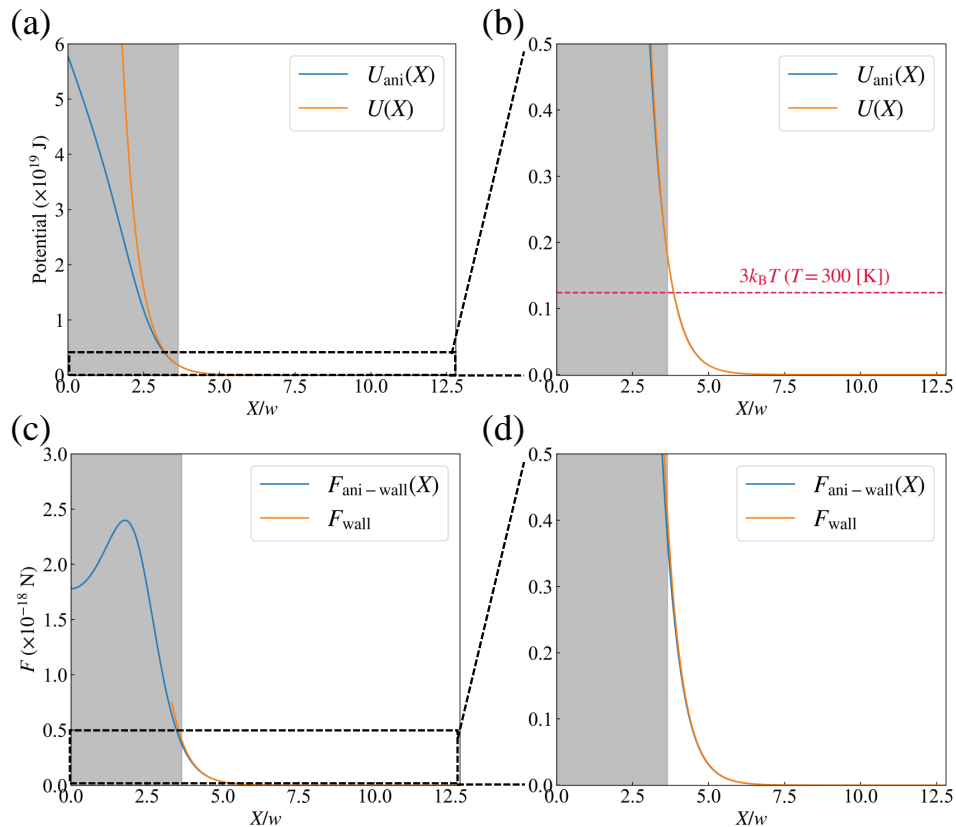


FIG. 6. (a), (b) Skyrmion potential formed by the magnetic anisotropy barrier and (c), (d) forces acting on the skyrmion. The blue and orange curves show the analytical equation and the model equation, respectively. (b) and (d) are enlarged views of (a) and (c), respectively. The gray areas in (b) and (d) are not considered in the simulations because of the large contribution from the corners.

- polymer, Proc. Natl. Acad. Sci. USA **105**, 9451 (2008).
- [4] K. Hayashi, H. Ueno, R. Iino, and H. Noji, Fluctuation theorem applied to f_1 -atpase, Phys. Rev. Lett. **104**, 218103 (2010).
- [5] T. Sagawa and M. Ueda, Second law of thermodynamics with discrete quantum feedback control, Phys. Rev. Lett. **100**, 080403 (2008).
- [6] T. Sagawa and M. Ueda, Minimal energy cost for thermodynamic information processing: Measurement and information erasure, Phys. Rev. Lett. **102**, 250602 (2009).
- [7] T. Sagawa and M. Ueda, Generalized jarzynski equality under nonequilibrium feedback control, Phys. Rev. Lett. **104**, 090602 (2010).
- [8] T. Sagawa and M. Ueda, Fluctuation theorem with information exchange: Role of correlations in stochastic thermodynamics, Phys. Rev. Lett. **109**, 180602 (2012).
- [9] T. Sagawa and M. Ueda, Role of mutual information in entropy production under information exchanges, New J. Phys. **15**, 125012 (2013).
- [10] J. Karbowski, Information thermodynamics: From physics to neuroscience, Entropy **26** (2024).
- [11] L. Szilard, Über die Entropieverminderung in einem thermodynamischen System bei Eingriffen intelligenter Wesen, Z. Phys. **53**, 840 (1929).
- [12] L. Brillouin, Maxwell's demon cannot operate: Information and entropy. I, J. Appl. Phys. **22**, 334 (1951).
- [13] C. H. Bennett, The thermodynamics of computation—a review, Int. J. Theor. Phys. **21**, 905 (1982).
- [14] R. Landauer, Irreversibility and heat generation in the computing process, IBM J. Res. Dev. **5**, 183 (1961).
- [15] T. Schreiber, Measuring information transfer, Phys. Rev. Lett. **85**, 461 (2000).
- [16] R. Kobayashi and K. Kitano, Impact of network topology on inference of synaptic connectivity from multi-neuronal spike data simulated by a large-scale cortical network model, J. Comput. Neurosci. **35**, 109 (2013).
- [17] M. Kawasaki, Y. Uno, J. Mori, K. Kobata, and K. Kitajo, Transcranial magnetic stimulation-induced global propagation of transient phase resetting associated with directional information flow, Front. hum. neurosci. **8** (2014).
- [18] M. Staniek and K. Lehnertz, Symbolic transfer entropy, Phys. Rev. Lett. **100**, 158101 (2008).
- [19] R. Vicente, M. Wibral, M. Lindner, and G. Pipa, Transfer entropy—a model-free measure of effective connectivity for the neurosciences, J. Comput. Neurosci. **30**, 45 (2011).
- [20] A. Roza, J. Morales, J. Moeyersons, R. Joshi, E. G. Ciani, P. Borzée, B. Buyse, D. Testelmans, S. Van Huffel, and C. Varon, Benchmarking transfer entropy methods for the study of linear and nonlinear cardio-respiratory interactions, Entropy **23** (2021).
- [21] O. Kwon and J.-S. Yang, Information flow between stock

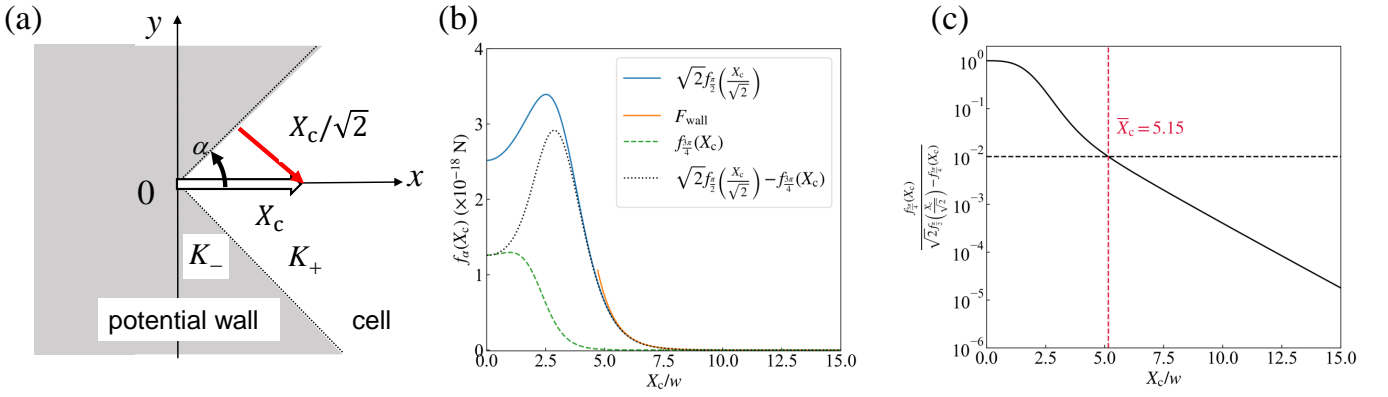


FIG. 7. Evaluation of forces acting from corner walls. (a) Coordinate system of the corner. Gray: magnetic anisotropic barrier. White: cell interior. (b) Forces acting from the wall. The blue and orange curves are the force $f_{\pi/2}$ from the wall and its model function F_{wall} at the corner angle $\alpha = \pi/2$, respectively. The green dashed and black dotted lines are the forces $f_{3\pi/4}$ and the difference between $f_{\pi/2}$ and $f_{3\pi/4}$. (c) Ratio of $f_{\pi/2}$ to $\sqrt{2}f_{\pi/2} - f_{3\pi/4}$. The ratio of forces at $X_c/w = 5.15$ is 10^{-2} .

- indices, *Europhys. Lett.* **82**, 68003 (2008).
- [22] R. Marschinski and H. Kantz, Analysing the information flow between financial time series: An improved estimator for transfer entropy, *Eur. Phys. J. B* **30**, 275 (2002).
- [23] O. Kwon and J.-S. Yang, Information flow between stock indices, *Europhys. Lett.* **82**, 68003 (2008).
- [24] L. Sandoval Jr, Structure of a global network of financial companies based on transfer entropy, *Entropy* **16**, 4443 (2014).
- [25] M. J. Falkowski and P. D. Domański, Causality analysis with different probabilistic distributions using transfer entropy, *Appl. Sci.* **13**, 5849 (2023).
- [26] W.-Q. Sun and D.-M. Yan, Identification of the nonlinear vibration characteristics in hydropower house using transfer entropy, *Nonlinear Dyn.* **75**, 673 (2014).
- [27] Y. Gao, X. Wang, T. Potter, J. Zhang, and Y. Zhang, Single-trial eeg emotion recognition using granger causality/transfer entropy analysis, *J. Neurosci. Methods* **346**, 108904 (2020).
- [28] R. Murcio, R. Morphet, C. Gershenson, and M. Batty, Urban transfer entropy across scales, *PLoS One* **10**, e0133780 (2015).
- [29] S. Ito, Backward transfer entropy: Informational measure for detecting hidden markov models and its interpretations in thermodynamics, gambling and causality, *Sci. Rep.* **6**, 36831 (2016).
- [30] M. Oka and T. Ikegami, Exploring default mode and information flow on the web, *PLoS One* **8**, e60398 (2013).
- [31] S. Ito and T. Sagawa, Information thermodynamics on causal networks, *Phys. Rev. Lett.* **111**, 180603 (2013).
- [32] T. H. R. Skyrme, A unified field theory of mesons and baryons, *Nucl. Phys.* **31**, 556 (1962).
- [33] U. K. Roessler, A. Bogdanov, and C. Pfeleiderer, Spontaneous skyrmion ground states in magnetic metals, *Nature* **442**, 797 (2006).
- [34] S. Mühlbauer, B. Binz, F. Jonietz, C. Pfeleiderer, A. Rosch, A. Neubauer, R. Georgii, and P. Böni, Skyrmion lattice in a chiral magnet, *Science* **323**, 915 (2009).
- [35] X. Yu, N. Kanazawa, Y. Onose, K. Kimoto, W. Zhang, S. Ishiwata, Y. Matsui, and Y. Tokura, Near room-temperature formation of a skyrmion crystal in thin-films of the helimagnet fege, *Nat. Mater.* **10**, 106 (2011).
- [36] T. Nozaki, Y. Jibiki, M. Goto, E. Tamura, T. Nozaki, H. Kubota, A. Fukushima, S. Yuasa, and Y. Suzuki, Brownian motion of skyrmion bubbles and its control by voltage applications, *Appl. Phys. Lett.* **114** (2019).
- [37] C. Schütte, J. Iwasaki, A. Rosch, and N. Nagaosa, Inertia, diffusion, and dynamics of a driven skyrmion, *Phys. Rev. B* **90**, 174434 (2014).
- [38] J. Zázvorka, F. Jakobs, D. Heinze, N. Keil, S. Kromin, S. Jaiswal, K. Litzius, G. Jakob, P. Virnau, D. Pinna, *et al.*, Thermal skyrmion diffusion used in a reshuffler device, *Nat. Nanotechnol.* **14**, 658 (2019).
- [39] S. Miki, Y. Jibiki, E. Tamura, M. Goto, M. Oogane, J. Cho, R. Ishikawa, H. Nomura, and Y. Suzuki, Brownian motion of magnetic skyrmions in one-and two-dimensional systems, *J. Phys. Soc. Jpn.* **90**, 083601 (2021).
- [40] L. Zhao, Z. Wang, X. Zhang, X. Liang, J. Xia, K. Wu, H.-A. Zhou, Y. Dong, G. Yu, K. L. Wang, *et al.*, Topology-dependent brownian gyromotion of a single skyrmion, *Phys. Rev. Lett.* **125**, 027206 (2020).
- [41] Y. Suzuki, S. Miki, Y. Imai, and E. Tamura, Diffusion of a magnetic skyrmion in two-dimensional space, *Phys. Lett. A* **413**, 127603 (2021).
- [42] Y. Jibiki, M. Goto, E. Tamura, J. Cho, S. Miki, R. Ishikawa, H. Nomura, T. Srivastava, W. Lim, S. Aufret, *et al.*, Skyrmion brownian circuit implemented in continuous ferromagnetic thin film, *Appl. Phys. Lett.* **117** (2020).
- [43] S. Miki, K. Hashimoto, J. Cho, J. Jung, C.-Y. You, R. Ishikawa, E. Tamura, H. Nomura, M. Goto, and Y. Suzuki, Spatial control of skyrmion stabilization energy by low-energy Ga⁺ ion implantation, *Appl. Phys. Lett.* **122** (2023).
- [44] R. Ishikawa, M. Goto, H. Nomura, and Y. Suzuki, Implementation of skyrmion cellular automaton using brownian motion and magnetic dipole interaction, *Appl. Phys. Lett.* **119** (2021).
- [45] S.-Z. Lin, C. Reichhardt, C. D. Batista, and A. Saxena, Particle model for skyrmions in metallic chiral magnets:

- Dynamics, pinning, and creep, *Phys. Rev. B* **87**, 214419 (2013).
- [46] D. Capic, D. A. Garanin, and E. M. Chudnovsky, Skyrmion–skyrmion interaction in a magnetic film, *J. Phys. Condens. Matter* **32**, 415803 (2020).
- [47] D. Pinna, F. Abreu Araujo, J.-V. Kim, V. Cros, D. Querlioz, P. Bessiere, J. Droulez, and J. Grollier, Skyrmion gas manipulation for probabilistic computing, *Phys. Rev. Appl.* **9**, 064018 (2018).
- [48] A. Thiele, Steady-state motion of magnetic domains, *Phys. Rev. Lett.* **30**, 230 (1973).
- [49] I. Makhfudz, B. Krüger, and O. Tchernyshyov, Inertia and chiral edge modes of a skyrmion magnetic bubble, *Phys. Rev. Lett.* **109**, 217201 (2012).
- [50] F. Büttner, C. Moutafis, M. Schneider, B. Krüger, C. Günther, J. Geilhufe, C. v. K. Schmising, J. Mohanty, B. Pfau, S. Schaffert, *et al.*, Dynamics and inertia of skyrmionic spin structures, *Nat. Phys.* **11**, 225 (2015).
- [51] Y. Suzuki, S. Miki, H. Nomura, and E. Tamura, Mass and generalized thiele equation of the magnetic skyrmion, arXiv:2208.01835 (2022).
- [52] E. Tamura, C. Liu, S. Miki, J. Cho, M. Goto, H. Nomura, R. Nakatani, and Y. Suzuki, Skyrmion confinement and dynamics in tracks patterned with magnetic anisotropy: theory and simulations, arXiv:2005.04860 (2020).
- [53] J. Cho, E. Tamura, C. Liu, S. Miki, C.-Y. You, J.-S. Kim, H. Nomura, M. Goto, R. Nakatani, and Y. Suzuki, Manipulating 1-dimensional skyrmion motion by the external magnetic field gradient, *New J. Phys.* **22**, 103053 (2020).
- [54] X. Wang, H. Yuan, and X. Wang, A theory on skyrmion size, *Commun. Phys.* **1**, 31 (2018).
- [55] A. Hrabec, J. Sampaio, M. Belmeguenai, I. Gross, R. Weil, S. M. Chérif, A. Stashkevich, V. Jacques, A. Thiaville, and S. Rohart, Current-induced skyrmion generation and dynamics in symmetric bilayers, *Nat. Commun.* **8**, 15765 (2017).
- [56] A. Belavin and A. Polyakov, Metastable states of two-dimensional isotropic ferromagnets, *JETP Lett.* **22**, 245 (1975).
- [57] S. Miki, E. Tamura, H. Nomura, M. Goto, and Y. Suzuki, Size-independent drive of one-dimensional skyrmion motion using exchange energy control, *J. Phys. Soc. Jpn.* **90**, 114703 (2021).
- [58] J. T. Lizier, M. Prokopenko, and A. Y. Zomaya, Local measures of information storage in complex distributed computation, *Inf. Sci.* **208**, 39 (2012).